Toward an Optimal Position for IVC Filters: Computational Modeling of the Impact of Renal Vein Inflow

S. L. Wang, M. A. Singer

July 13, 2009

Disclaimer

This document was prepared as an account of work sponsored by an agency of the United States government. Neither the United States government nor Lawrence Livermore National Security, LLC, nor any of their employees makes any warranty, expressed or implied, or assumes any legal liability or responsibility for the accuracy, completeness, or usefulness of any information, apparatus, product, or process disclosed, or represents that its use would not infringe privately owned rights. Reference herein to any specific commercial product, process, or service by trade name, trademark, manufacturer, or otherwise does not necessarily constitute or imply its endorsement, recommendation, or favoring by the United States government or Lawrence Livermore National Security, LLC. The views and opinions of authors expressed herein do not necessarily state or reflect those of the United States government or Lawrence Livermore National Security, LLC, and shall not be used for advertising or product endorsement purposes.

Toward an Optimal Position for IVC Filters: Computational Modeling of the Impact of Renal Vein Inflow

Authors: Stephen L.Wang, MD (1)* and Michael A. Singer, PhD (2)

(1) Division of Vascular and Interventional Radiology
     Kaiser Permanente Santa Clara
     Santa Clara, CA 95051

(2) Center for Applied Scientific Computing
     Lawrence Livermore National Laboratory
     Livermore, CA 94551

*Corresponding Author

ABSTRACT

Purpose: To evaluate the hemodynamic effects of renal vein inflow and filter position on unoccluded and partially occluded IVC filters using three-dimensional computational fluid dynamics.

Materials and Methods:
Three-dimensional models of the TrapEase and Gunther Celect IVC filters, spherical thrombi, and an IVC with renal veins were constructed. Hemodynamics of steady-state flow was examined for unoccluded and partially occluded TrapEase and Gunther Celect IVC filters in varying proximity to the renal veins.

Results:
Flow past the unoccluded filters demonstrated minimal disruption. Natural regions of stagnant/recirculating flow in the IVC are observed superior to the bilateral renal vein inflows, and high flow velocities and elevated shear stresses are observed in the vicinity of renal inflow. Spherical thrombi induce stagnant and/or recirculating flow downstream of the thrombus. Placement of the TrapEase filter in the suprarenal vein position resulted in a large area of low shear stress/stagnant flow within the filter just downstream of thrombus trapped in the upstream trapping position.

Conclusions:
Filter position with respect to renal vein inflow influences the hemodynamics of filter trapping. Placement of the TrapEase filter in a suprarenal location may be thrombogenic with redundant areas of stagnant/recirculating flow and low shear stress along the caval

wall due to the upstream trapping position and the naturally occurring region of stagnant flow from the renal veins. Infrarenal vein placement of IVC filters in a near juxtarenal position with the downstream cone near the renal vein inflow likely confers increased levels of mechanical lysis of trapped thrombi due to increased shear stress from renal vein inflow.

INTRODUCTION

Inferior vena cava (IVC) filters have played an integral role in the prevention of pulmonary embolism from deep venous thrombosis for over 30 years. Over 100,000 filters are placed annually in the US alone (1). Despite this extensive utilization of filters, very little is understood about the ideal position for an IVC filter. Currently, IVC filter manufacturers have received approval for filter placement only in the infrarenal IVC, though off-label use in the suprarenal IVC with particular clinical scenarios (e.g., thrombus in the gonadal or renal veins, thrombus within the IVC at or near the level of the renal veins, anatomic variation in IVC and renal vein, and intrinsic or extrinsic IVC narrowing) is well-documented (2).

An ideal IVC filter traps significant thrombus without significantly increasing the risk of thrombosis from either inducing a prothrombotic state or from trapping emboli. Most endovascular interventionalists advocate filter placement in an infrarenal position,

thereby decreasing the risk of renal vein thrombosis from potential filter occlusion. The "infrarenal" portion of the IVC is a vague term that includes the entire length of the IVC from the renal veins caudally to the IVC bifurcation into the common iliac veins. With respect to renal vein inflow, where is the precise, ideal position to deploy an IVC filter? Does such a location exist?

The Society of Interventional Radiology Foundation consensus panel on the development of research agenda for IVC filters recently published a list of basic science research priorities which includes "computerized flow dynamic studies of multiple filters." (3). Both in vitro bench experiments and computational flow modeling of several types of filters have been reported (4-7). However, no prior study has incorporated renal vein inflow. Building on the work of Singer et al., which evaluated the TrapEase IVC filter in a computational flow model and corroborated results with bench experiments (6), this study models the TrapEase (Cordis, Miami Lakes, FL) and Gunther Celect filters (Cook, Bloomington, IN) with and without nonocclusive thrombus in an IVC model that incorporates anatomically correct renal vein inflows. Computer simulations were run with the filters in varying proximity to the renal veins to determine whether an ideal position with regard to renal vein inflow and filter flow dynamics exists.

MATERIALS AND METHODS

Three-dimensional computer models of the IVC with renal veins, Gunther Celect filter, TrapEase filter, and simulated thrombi were constructed to study flow dynamics with the

filters in various positions. Hemodynamics in and around unoccluded and partially occluded filters was examined using three-dimensional computational fluid dynamics.

IVC and Renal Vein model:
As previously described by Singer et al. (6), the IVC was modeled as a rigid, straight pipe with a diameter of 23 mm, per the average IVC diameter described by Kaufman et al. (8). Renal veins were also modeled as straight rigid pipes.

The diameters and entry angles of the renal veins into the IVC were calculated from abdominal CT scans of 24 patients (12 males, 12 females; average age 55, age range 16-89) with no known renal disease or variant renal venous anatomy. Renal veins diameters were measured from IV contrast enhanced 2.5 mm slice thickness axial CT images (GE Lightspeed 16; Milwaukee, WI) near the confluence with the IVC. Renal vein entry angles were measured using PACS software (Stentor I-site,ver 3.3.1, Philips, The Netherlands) from IV contrast enhanced 5 mm slice thickness coronal CT images reformatted from the axial source images. Coronal reformatted images were also used to identify which renal vein was more caudal in location, and the cranio-caudal distance between the right and left renal veins was recorded. Average bilateral renal vein diameters (right = 10.5 mm +/- 2.0 mm, left = 8.8 mm +/- 1.8 mm), bilateral renal vein entry angles (right= 62.0 degrees +/- 26.8 degrees, left = 60.7 degrees +/- 11.1 degrees), and cranial caudal distance between the renal vein entry levels (6.8 mm +/- 7.5mm) were used to construct the model of the IVC and renal veins. The right renal vein was more caudal than the left in a majority of the patients (right more caudal n=10, left more caudal n=3, approximately same level n= 11).   Therefore, the model was constructed with the right renal vein entry 10mm more caudal than the left.

Patient anatomic information utilized from the CT scans was given exemption status after meeting our Institutional Review Board and federal regulatory criteria for exemption.

TrapEase and Gunther Celect Filter models:
Construction of the TrapEase model was described in (6). The computer model of the Gunther Celect filter was similarly constructed using methods of computer aided design. In particular, the Celect filter was inserted into a 23 mm inner diameter glass test tube and high resolution digital photographs were taken using a Dimage Xt digital camera (Minolta, Osaka, Japan). Measurements of the filter were also obtained using a Cen-tech 6 inch digital caliper (Harbor Freight Tools, Camarillo, CA). The photographs and measurement data were then imported into the GNU Image Manipulation Program (GIMP) (available at http://www.gimp.org) where spatial geometry of the filter was

extracted on the basis of pixel color and location. The geometric specifications were imported into the Overture software framework (Lawrence Livermore National Laboratory, Livermore, CA, available for download at http://computation.llnl.gov/casc/Overture) (9,10), where computer models were constructed for each filter. For ease in modeling, the extraluminal barbs were excluded from the model because the presence does not alter the characteristics of flow intraluminally.

Clot Models:
As previously described by Singer et al.(6), spherical thrombi were modeled as rigid spheres. The volumes were 0.5 and 1.0 –mL, which is consistent with the visual scale described by Wang et al. and similar to the volumes used in previous studies using the TrapEase filter (11).

Simulations:
As previously described by Singer at al.(6), flow was modeled as an incompressible, Newtonian fluid whose motion is described mathematically by the Navier-Stokes equation (12). The Navier-Stokes equations were solved by using the incompressible flow solver within the Overture software framework, and postprocessing was performed using tools provided by Overture, custom scripts written in Matlab (Mathworks, Natick, Massachusetts), and the GIMP.

Simulations were performed with unoccluded and partially occluded TrapEase and Gunther Celect filters. Thrombi were positioned in the upstream and downstream trapping positions of the TrapEase filter and in the single, downstream position of the Gunther Celect filter. Both filters were placed in the geometric center of the simulated cylindrical IVC and were placed in varying locations in the cranial-caudal plane of the IVC to simulate infrarenal vein placement (Fig. 1, positions A and B), juxtarenal vein placement (positions C, D, and E), as well as suprarenal vein placement (position F).

The mean inlet velocity of the infrarenal vein IVC was 3.44 cm/sec, which corresponds to a flow rate of 0.86 L/min in the 23 mm diameter IVC and a Reynold's number (Re) of 320 (Re= $\rho U D / \mu$ where ρ is the density of blood (1,040 kg/m3), U is the mean inlet velocity, D is the diameter of the vena cava [23 mm], and μ is the viscosity of blood [2.57 e-3kg/msec]). Though a Re of 600 has been used in previous studies (4, 6, 7, 13), the corresponding flow rate (e.g., 2 L/min in a 2 cm vena cava [4]) is more indicative of higher flow velocity typically seen in the suprarenal IVC. The peak renal vein flow velocities were 40.2 cm/sec and 43.5 cm/sec for the right and left veins, respectively.

These velocities are consistent with previous reports of doppler renal vein velocities in normal adults (14). Inflow to the IVC and renal veins was specified by parabolic velocity profiles.

RESULTS

As in Singer et al. (6), the three-dimensional Navier-Stokes equations were solved for the velocity and the pressure. In the contour plots of the axial velocity, all velocities were normalized by the corresponding value for fully developed pipe flow. Because the speed of renal inflow is significantly greater than IVC flow (as noted above), the color scales show the greatest variation of flow speeds near the renal veins: flow upstream of the renal veins is relatively uniform. The wall shear stresses were normalized by the corresponding value for pipe flow, and the breaks in the line plots denote the locations of renal inflow, where no wall is present. In all figures, IVC flow is bottom to top, and renal vein flow is towards the cava.

Unoccluded filters

For the unoccluded TrapEase and Celect filters (Fig. 2), there is minimal disruption to the flow upstream of the renal veins. That is, using the velocity scales that capture the dynamics of the renal inflow, both filters demonstrate only small deviation from pipe flow. Near the sites of renal inflow, the renal veins act as jets that introduce high speed flow into the cava, and the flow downstream of the renal veins is disrupted. Immediately downstream of both renal veins, regions of low velocity and recirculating flow are observed near the wall of the cava, which is due to the large velocity difference between IVC flow and renal flow (arrows, Fig. 2). The filters disrupt the renal inflow in close proximity to the renal veins; the flow must change direction (thereby increasing the transverse components of velocity) in order to by-pass the filter and flow downstream. When the filter is proximal to or downstream of the renal veins, flow inside the filter is disrupted significantly.

The wall shear stress profiles for both unoccluded filters exhibit regions of low WSS immediately downstream of the renal inflow (dotted lines in Fig. 5, 9, 10). As noted above, these areas correspond to regions of low velocity flow that is pushed aside by high velocity flow coming from the renal veins. Consequently, the recirculating flow gives rise to negative velocity gradients, which produce large, negative wall shear stresses. Upstream of the renal inflow, the wall shear stresses are nearly uniform, and the

normalized values are close to unity thereby indicating minor deviations from pipe flow.

Partially occluded filters

Partial occlusion of the TrapEase and Celect filters disrupts flow downstream of the thrombus. When trapped thrombus is proximal to the renal veins, however, incoming renal flow is redirected by the thrombus and forced downstream along the cava wall. Consequently, flow along the cava wall (immediately downstream of renal inflow) is accelerated, and the volume of stagnant/recirculating flow, in comparison to the unoccluded configuration, is reduced. In addition, the incoming renal vein flow may be directed at the downstream trapped thrombus when the filter cones are positioned closer to the renal veins.

As previously described by Singer et al. (6), partially occlusive thrombus in the upstream trapping position of the TrapEase results in a region of low-speed, intrafilter flow (Figs. 6-8) that is accompanied by low shear stresses along the ipsilateral cava wall (Fig. 10). This region of stagnant/recirculating flow can be larger when the TrapEase is placed in a suprarenal location, as the stagnant region along the cava wall due to the non-occlusive thrombus overlaps with a naturally occurring region of stagnant/recirculating flow just downstream to the renal vein inflow bilaterally (Fig. 10).

Wall shear stress profiles for the two filters are qualitatively similar (Figs. 5,9, and 10). In particular, for the filters upstream or inferior to the renal veins, the peak wall shear stress occurs near the narrow passage between the cava wall and the trapped thrombus; the minimum wall shear stress is near the stagnant/recirculating zone immediately downstream of renal inflow. When the filters are in a suprarenal vein location, the locations of maximum and minimum wall stress remain unchanged (near the thrombus and downstream of renal inflow, respectively), but the trapped thrombus is downstream of renal inflow, which leads to a comparatively large peak in the wall shear stress due to the high speed flow past the thrombus.

DISCUSSION

Our computational flow study indicates that renal vein inflow has significant hemodynamic effects on blood flow near IVC filters. Based on prior MRI and ultrasound studies that included groups of control patients (14-16), there is some variability in peak

renal venous velocities. The renal inflow velocities used here fall well-within the parameters from prior physiological studies. The renal venous flow in the model dominates the overall flow pattern in the IVC downstream from the renal inflow. This dominant flow is perhaps best demonstrated by a naturally occurring region of stagnant/recirculating flow, which is superior to the confluence of each renal vein (arrows, Figs. 2, and 8).

Singer et al. previously demonstrated intrafilter regions of low shear stress and stagnant/recirculating flow along the cava wall, immediately downstream of the upstream trapping position of the TrapEase (6). Regions of low shear stress and stagnant/recirculating flow can be thrombogenic due to the accumulation of thrombin and fibrin (17). Recent clinical studies suggest a higher incidence of intrafilter thrombus and caval thrombosis with the near structurally identical OptEase filter as described by Singer et al. (6) The upstream trapping position is particularly concerning with the TrapEase filter in a suprarenal position since the region of stagnant/recirculating flow just downstream of trapped thrombus in the upstream trapping position can overlap with the naturally occurring region of stagnant/recirculating flow just superior to renal vein confluence bilaterally (Figs. 8 and 10). If the two regions overlap, the portion of vessel occupied by stagnant flow is larger and may increase the risk for thrombosis along the caval wall.

This study presents results from the first published computational flow model of the Gunther Celect filter. In its optimal position, which is centered in the IVC, the Celect filter demonstrates minimal flow disturbance in the unoccluded state. Since the Celect has only one trapping position, the resulting flow dynamics are similar to the downstream trapping position of the TrapEase filter. Both partially occluded filters demonstrated similar regions of low shear stress and stagnant flow downstream from the simulated thrombi. High shear stress is seen along the caval wall downstream from the thrombus in the infrarenal filter positions. As both filters are moved more superiorly, with the downstream capture cone just below or near the level of the renal vein inflow (positions B and C), the volume of stagnant/recirculating flow downstream from the filter decreases. In addition, very high velocities and shear stresses are seen along the downstream filter cone. These conditions may reduce the risk of primary hemostasis by stimulating the secretion of tissue plasminogen activator and therefore reduce the risk of secondary hemostasis by clearing fibrin and thrombin and increasing mechanical lysis of thrombi (18). Thus, placement of these two IVC filters in a near juxtarenal location (positions B and C) may decrease the risk of thrombus propagation within the filter cone as

significantly higher shear stresses and velocities from renal vein inflow serve to reduce stagnant flow and may improve mechanical lysis of trapped thrombi.

Positioning the filters in a true juxtarenal position (position D) results in similar regions of high shear stress and velocities in the central, downstream trapping positions of both filters. Though this may also serve to mechanically lyse smaller thrombi trapped in the filter, positioning the filter at this level must be weighed against the risk of caval occlusion (possibly from large, unstable lower extremity deep venous thrombus) and potential subsequent bilateral renal vein occlusion. In addition, the legs and centering struts of the Celect may become engaged in the renal veins.

Suprarenal placement of the filters demonstrates the dominant flow of the renal veins relative to flow through the IVC. High shear stresses and velocities are seen along the caval walls in the partially occluded TrapEase and Celect filters in the downstream positions. In the case of partially occluded filters, the significantly increased flow rates and shear stresses along the caval walls would suggest a decreased risk of secondary hemostasis due to mechanical lysis and clearing of fibrin and thrombin. A recent retrospective, single center review of suprarenal filters (n=70) by Kalva et al. had no patients present with caval thrombosis with mean follow up of 573 days; however, it is worth noting that in the 30 patients who had follow up abdominal CT scans, intrafilter thrombus was noted in 3 cases (10%), two TrapEase and one Gunther Tulip (Cook, Bloomington, IN) (2). Furthermore, the thrombus was "seen in the periphery of the TrapEase filter as a thin rim attached to the wall of the IVC. In the case of the Tulip filter, the thrombus was seen in the apex of the filter…" These clinical observations regarding the location of trapped thrombus correlate well with results from our flow models. Specifically, trapped thrombus in the upstream trapping position of the TrapEase filter may induce a larger region of stagnant flow along the ipsilateral cava wall due to a naturally occurring region of stagnant flow that is already present due to renal inflow. This could lead to intrafilter thrombus along the cava wall, which may be difficult to clear due to stagnant flow. This correlates with what was described clinically by Kalva, et al.

Our computer model is founded on simplifying but generally realistic assumptions. The walls of the vena cava and renal veins are modeled as smooth and rigid, though in vivo the vena cava and renal veins are dynamic and demonstrate variations in angle and radial diameter. Our steady-state flow velocities from the renal veins and IVC are based on clinical studies from MRI and ultrasound (14-15), but in vivo the inflow velocities are unsteady and change with exercise and physiological conditions. This

study is limited to spherical thrombi, but based on results from Singer et al., different shapes generally result in similar shear stresses and velocity profiles, especially when thrombi are trapped in the center of the IVC (6). Swaminathan also noted that spherical thrombi represent, in some sense, a statistical average of irregular shapes. (19) Renal vein diameters and angles are based on average values from patient CT scans, though significant variation is seen within the general population and renal venous anatomic variants are common (circumaortic left renal vein, retroaortic left renal vein, and duplicated IVCs) (20). Other sources of IVC inflow including lumbar veins and other venous tributaries are not included in our model. Finally, the Celect filter was modeled only in the center of the IVC, but the Celect is susceptible to tilting at the time of deployment (21).

Our computational flow model of the IVC and renal veins suggests that the ideal location for infrarenal IVC filter placement is immediately upstream of the juxtarenal position, with the downstream cone of the filter near the level of renal inflow (Position C). The dominating high velocity flow from the renal veins serves as a source of higher shear stresses and flow velocities that may decrease primary and secondary hemostasis, particularly in the case of nonocclusive thrombi trapped in the downstream filter cone. True juxtarenal positioning confers similar higher shear stresses but also increases the risk of renal vein thrombosis from filter occlusion. Suprarenal placement of IVC filters may confer a decreased risk of hemostasis due to much higher wall shear stress and flow velocities; however, in the event of a large occlusive thrombus, the risk of renal vein thrombosis must be considered. Suprarenal placement of the TrapEase filter carries the additional risk of inducing large, redundant areas of stagnant flow at the upstream trapping position that may be thrombogenic. Given the results of this computational flow model, future clinical studies of IVC filters that examine outcomes based on the relative position of filters with regard to renal veins are warranted.

REFERENCES:

1. Lee P, Raizada A, Ciocca R. Growing utilization of IVC filter placement from 2001-2005: Analysis of NIS. Abstract for the Society for Clinical Vascular Surgery 2009 Meeting; Available at: http://scvs.vascularweb.org/SCVS_Contribution_Pages/Abstracts/2009/MP26.html. Accessed January 22, 2009.

2. Kalva SP, Chlapoutaki CC, Wicky, S, et al. Suprarenal inferior vena cava filters: a 20-year experience. J Vasc Intervent Radiol 2008; 19: 1041-1047.

3. Kaufman JA, Rundback JH, Kee ST, et al. Development of a research agenda for inferior vena cava filters: Proceedings from a multidisciplinary research consensus panel. J Vasc Intervent Radiol 2009; 20: 697-707.

4. Leask RL, Johnston KW, Ohja M. Hemodynamic effects of clot entrapment in the TrapEase inferior vena cava filter. J Vasc Intervent Radiol 2004; 15:485-490.

5. Stewart SF, Robinson RA, Nelson, RA, et al. Effects of thrombosed vena cava filters on blood flow: flow visualization and numerical modeling. Ann Biomed Eng 2008; 36: 1764-1781.

6. Singer MA, Henshaw WD, and Wang, SL Computational modeling of blood flow in the TrapEase inferior vena cava filter. J Vasc Intervent Radiol 2009; 20: 799-805.

7. Harlal A, Ojha M, Johnston KW. Vena cava filter performance based on hemodynamics and reported thrombosis and pulmonary embolism patterns. J Vasc Interv Radiol 2007; 18:103-115.

8. Kaufman, JA, Waltman, AC, Rivitz, SM, Geller SC. Anatomical observations on the renal veins and inferior vena cava at magnetic resonance angiography. Cardiovasc Intervent Radiol 1995; 18:153-157.

9. Brown DL, Henshaw WD, Quinlan DJ. An object oriented framewoek for solving partial differential equations. In :Scientific Computing in Object-Oriented Parallel Environments, Springer Lecture Notes in Computer Science, 1997; 1343:177-194.

10. Henshaw, WD, Schwendeman DW. Moving overlapping grids with adaptive mesh refinement for high speed reactive and non-reactive flow. J Comp Phys 2006; 216: 744-779.

11. Wang SL, Timmermans HA, Kaufman JA. Estimation of trapped thrombus volumes in retrievable inferior vena cava filters: a visual scale. J Vasc Interv Radiol 2007; 18:273-276.

12. Panton RL. Incompressible Flow, In: Incompressible Flow, 2nd ed. New York: John Wiley & Sons, Inc., 1996; 228-253.

13.Leask RL, Johnston KW, Ojha M. In vitro hemodynamic evaluation of a Simon nitinol vena cava filter: possible explanation of IVC occlusion. J Vasc Interv Radiol 2001; 12:613-618.

14. Avasthi PS, Greene ER, Scholler C, et al. Noninvasive diagnosis of renal thombosis by ultrasonic echo-doppler flowmetry. Kidney Int 1983: 882-887.

15. Cheng CP, Herfkens RJ, Taylor CA. Inferior vena cava hemodynamics quantified in vivo at rest and during cyclic exercises using magnetic resonance imaging. Am J Physiol Heart Circ Physiol 2003; 284:1161-1167.

16. Kim WS, Cheon JE, Kim IO, et al. Hemodynamic investigation of the left renal vein in pediatric varicocele: Doppler US, venography, and pressure measurements. Radiology 241: 228-234.

17. Lowe G. Virchow's triad revisited: abnormal flow. Pathophysiol Haemost Thromb 2003/2004; 33: 455-457.

18. Kroll MH, Hellums JD, Mcintire LV, Schafer AI, Moake, JL. Platelets and shear stress. Blood 1996; 88: 1525-1541.

19. Swaminathan TN, Hu HH, Patel AA. Numerical analysis of the hemodynamics and embolus capture of a Greenfield vena cava filter. J Biomed Eng 2006; 128:360-370.

20. Trigaux JP, Vandrogogenbroek S, De Wispelaere JF, et al. Congenital anomalies of the inferior vena cava and left renal vein: Evaluation with spiral CT. J Vasc Interv Radiol 1998; 9:339-345.

21. Smouse HB, Van Alstine WG, Mack S, et al. Deployment performance and retrievability of the Cook Celect vena cava filter. J Vasc Interv Radiol 2009; 20: 376-383.

FIGURES:

F

downstream

E

D

127°

C

126.2°

10.5mm

8.79mm

B

left
renal
vein

right
renal
vein

A
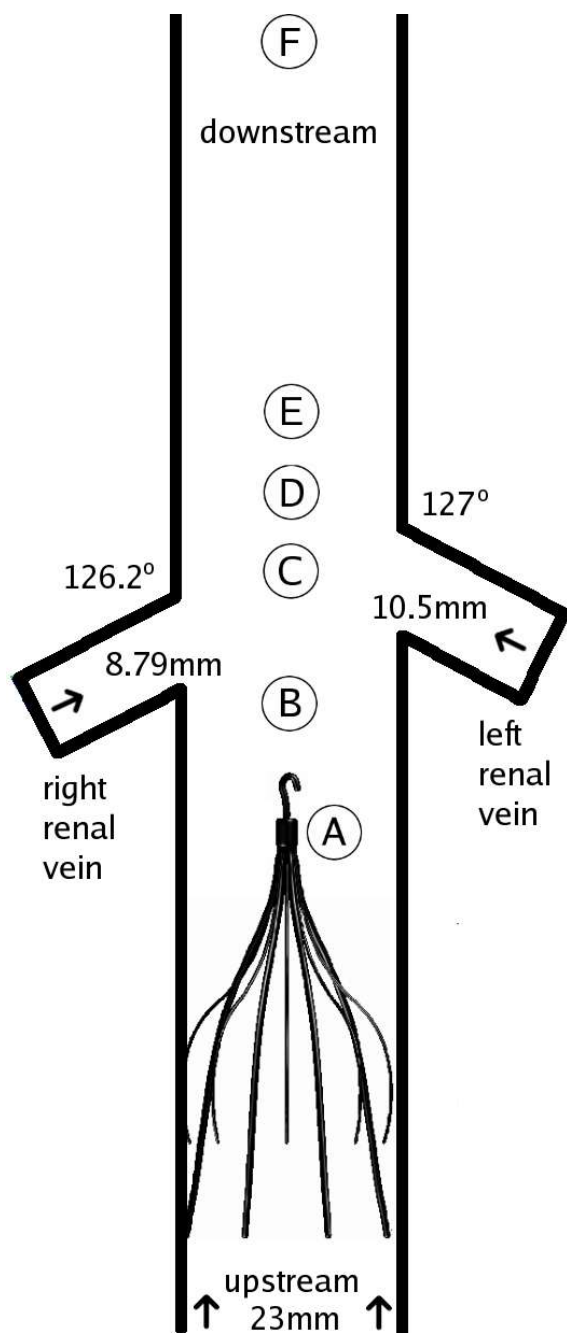
upstream
23mm

Figure 1

Figure 1: Schematic diagram of the IVC and renal vein three-dimensional model with filter positions labeled. Letters A-F correspond with position of the downstream cone of the Celect and TrapEase filters. Positions A and B are infrarenal, C is just below juxtarenal position with the cone near the level of the renal vein inflow, D and E are juxtarenal, and F is suprarenal in position.
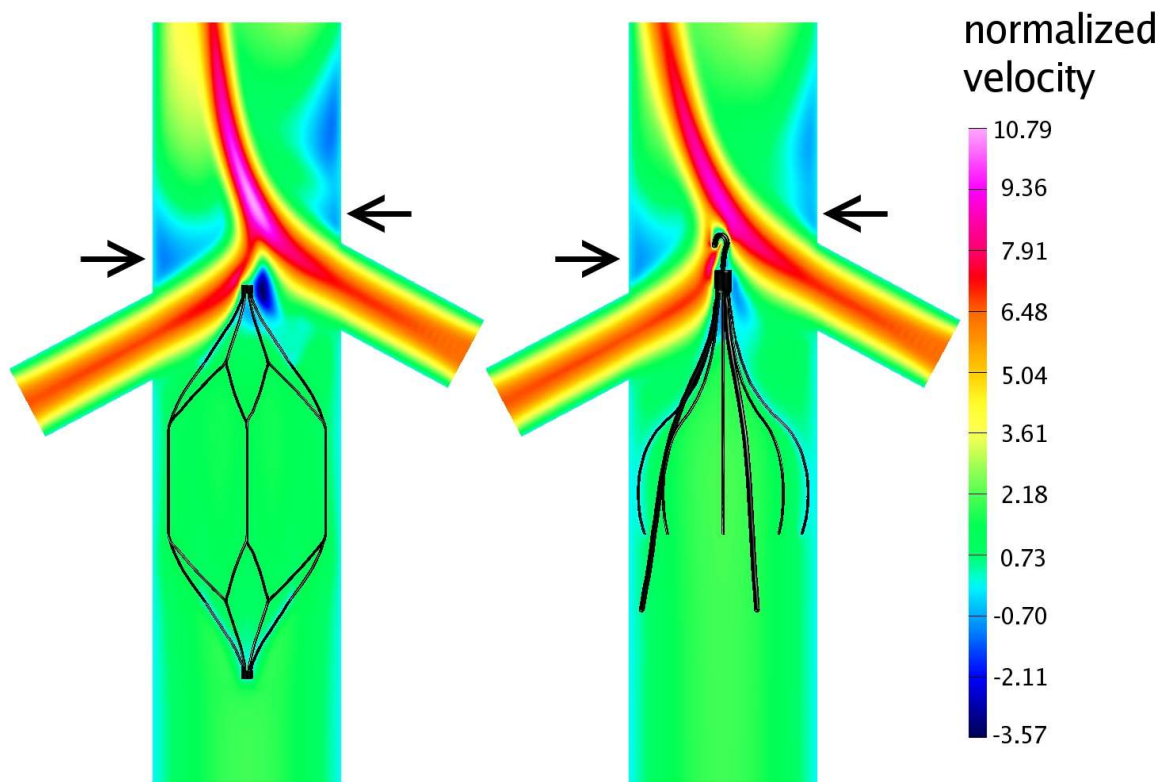
Figure 2

Figure 2: Models of unoccluded TrapEase and Celect filters within the IVC and renal vein computational flow model. Filters are positioned at vena cava position C (see schematic diagram, Fig. 1) Note the regions (arrows) of naturally occurring stagnant flow along the bilateral cava walls just downstream of the renal venous inflow.
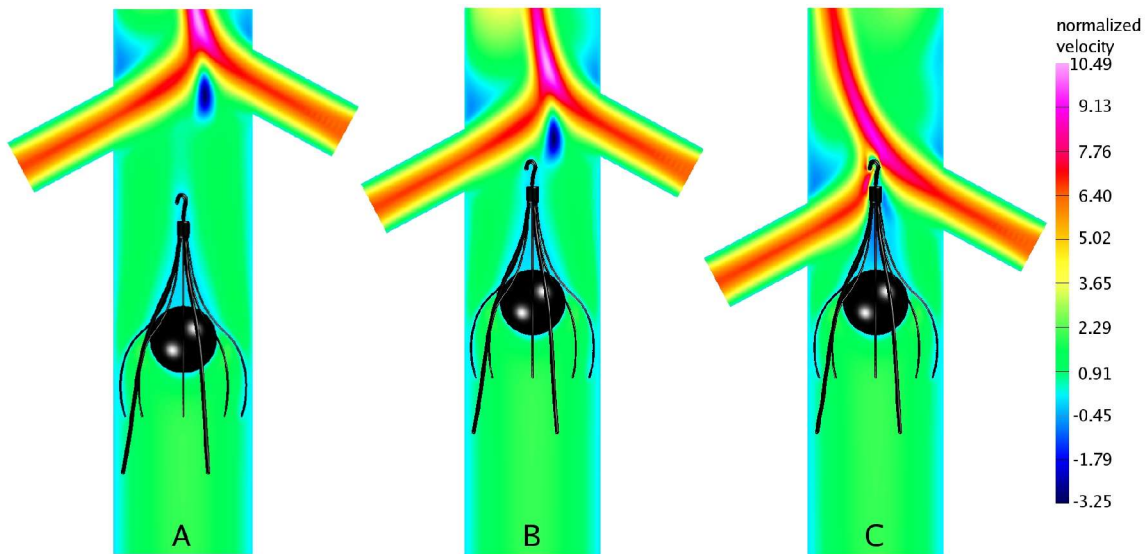
Figure 3

Figure 3: Celect filter flow modeling with trapped 1.0cc thrombus with normalized velocity color scale. The filters are positioned in vena cava stations A-C corresponding with filter cone locations from schematic diagram (Fig. 1).
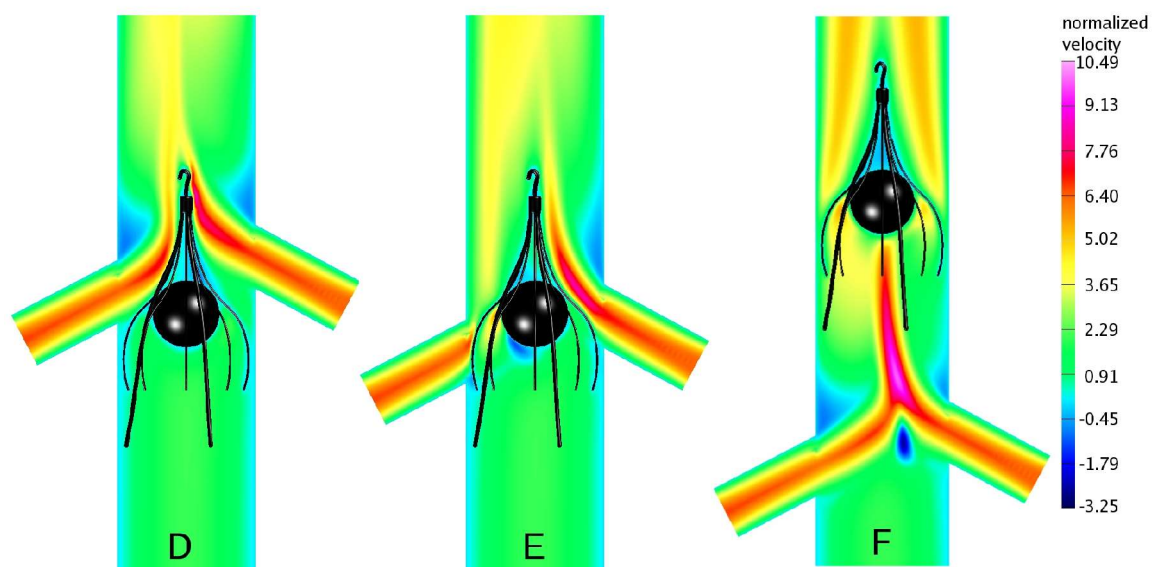
Figure 4

Figure 4: Celect filter in vena cava positions corresponding with stations D-F from Fig. 1.
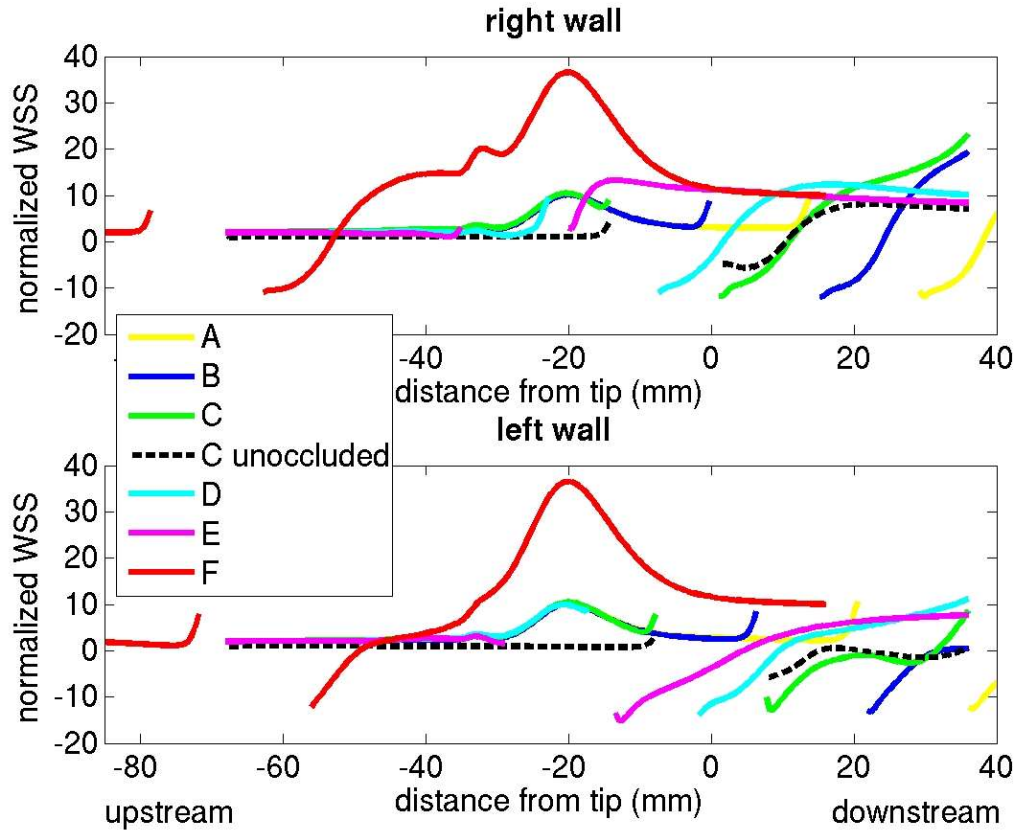Color scale corresponds with normalized velocities.

Figure 5

Figure 5: Normalized wall shear stress contours for the Celect filter in different IVC positions (A-F, see Fig. 1) with a 1 cc spherical thrombus in the central downstream trapping position. Dotted line indicates Celect filter at position C without thombus. Both sides of the cava wall are evaluated. Flow is left to right. X-axis denotes distance (in mm) from the downstream tip of the filter. Relative flow symmetry is observed in the Celect filter with low wall shear stress downstream of the thrombus and relatively high shear stress with suprarenal placement (position F). Breaks in wall shear stress lines correspond with position of renal vein inflow where no wall is present.
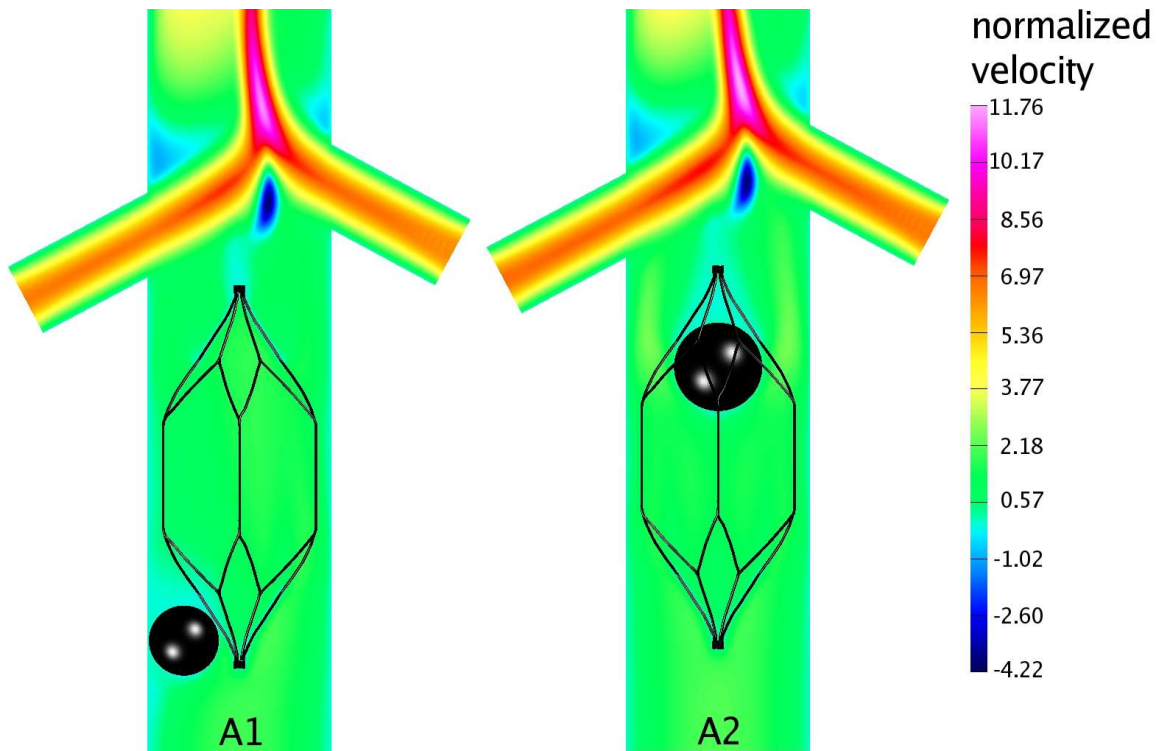
Figure 6

Figure 6: TrapEase filter at infrarenal vena cava station A (refer to schematic Fig. 1) with 0.5 cc simulated thrombus in the upstream trapping position (A1) and 1.0 cc simulated thrombus in the downstream trapping position (A2). Color scale corresponds with normalized velocities.
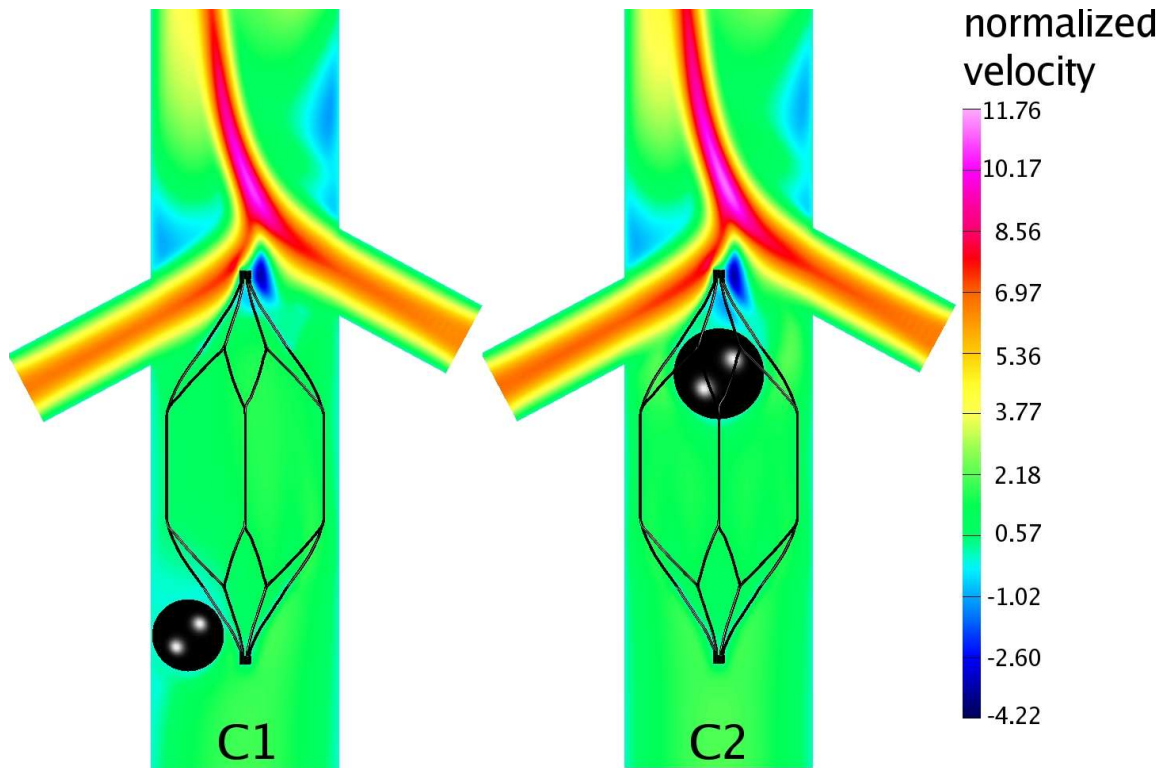
Figure 7

Figure 7: TrapEase filter at vena cava position C (refer to schematic Fig. 1) with 0.5 cc simulated thrombus in the upstream trapping position (C1) and 1.0 cc simulated thrombus in the downstream trapping position (C2). Color scale corresponds with normalized velocities.
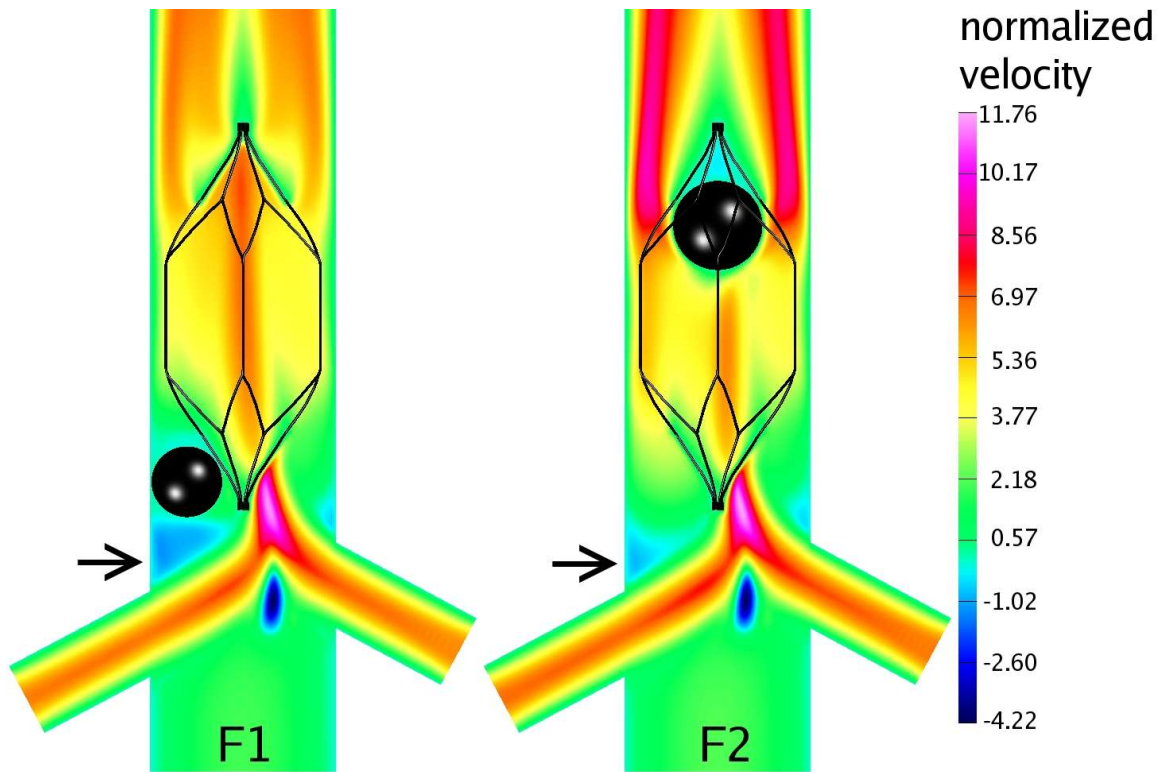
Figure 8:

Figure 8: TrapEase filter at suprarenal vena cava position F (refer to schematic Fig. 1) with 0.5 cc simulated thrombus in the upstream trapping position (F1) and 1.0 cc simulated thrombus in the downstream trapping position (F2). Color scale corresponds with normalized velocities. Arrows denote the naturally occurring regions of recirculating and/or stagnant flow due to renal vein inflow.
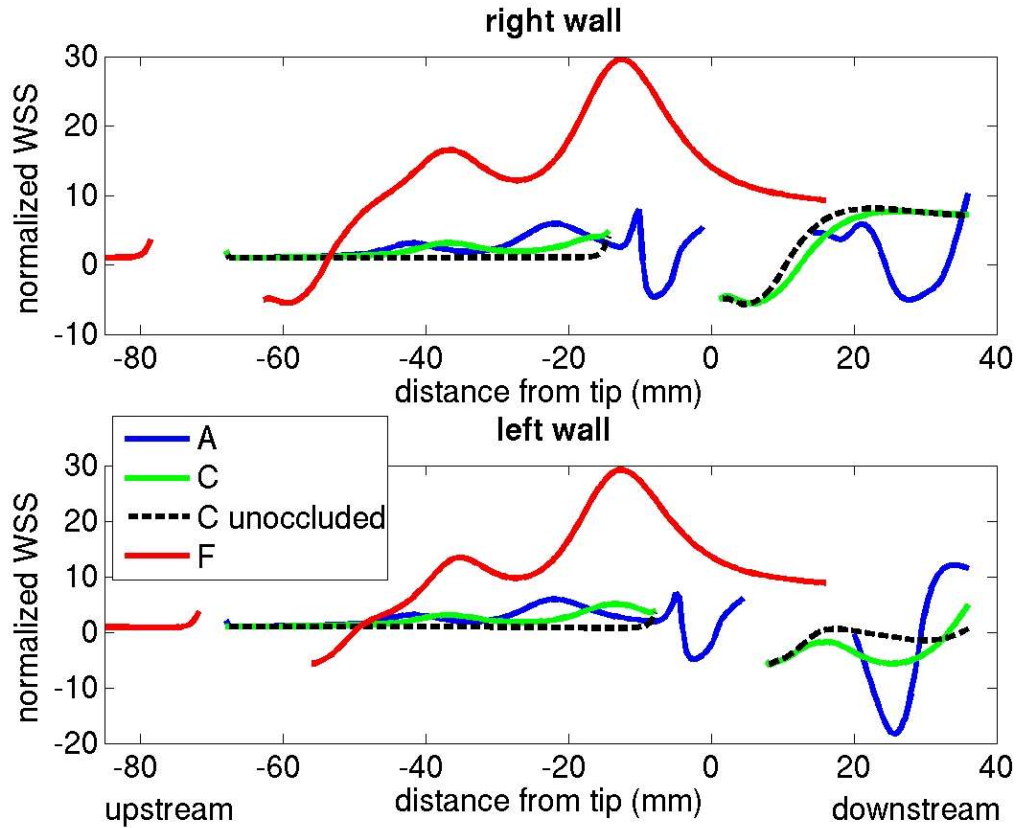
Figure 9

Figure 9: Normalized wall shear stress contours for the TrapEase filter in different IVC positions (A-F, see Fig. 1) with a 1 cc spherical thrombus in the central downstream trapping position. Dotted line indicates TrapEase filter at position C without thombus. Both sides of the cava wall are evaluated. Flow is left to right. X-axis denotes distance (in mm) from the downstream tip of the filter. Relative flow symmetry is observed in the TrapEase filter with low wall shear stress downstream of the thrombus and relatively high shear stress with suprarenal placement (position F). Breaks in wall shear stress lines correspond with position of renal vein inflow where no wall is present.
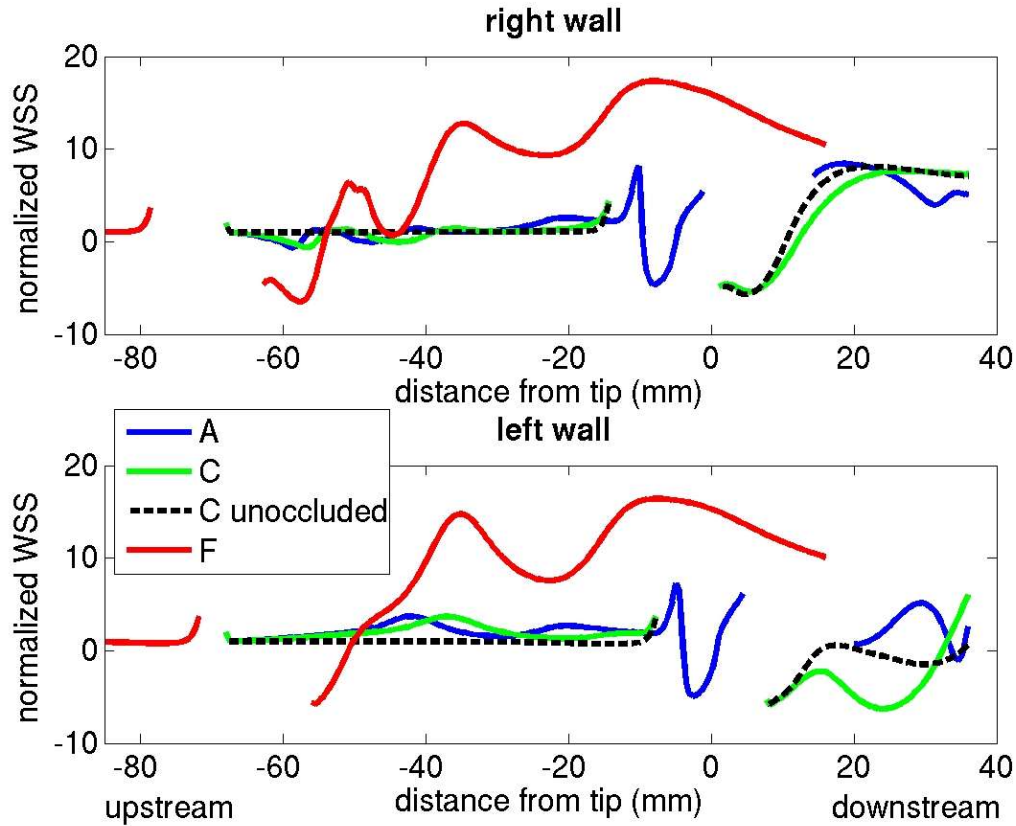
Figure 10

Figure 10: Normalized wall shear stress contours for the TrapEase filter in different IVC positions (A-F, see Fig. 1) with a 0.5 cc spherical thrombus in the right lateral upstream trapping position. Dotted line indicates TrapEase filter at position C without thombus. Both sides of the cava wall are evaluated. Flow is left to right. X-axis denotes distance (in mm) from the downstream tip of the filter. Note that at position F (red line) there is a drop in the right wall shear stress at approximately 50 cm proximal to the downstream tip of the filter. This is due to the upstream, laterally trapped thrombus which briefly overlaps with a naturally occurring region of stagnant and/or recirculating flow (from 55 to 60 cm upstream from the tip) due to renal vein inflow. Breaks in wall shear stress lines correspond with position of renal vein inflow where no wall is present.